2022 IEEE 16th International Conference on Solid-State & Integrated Circuit Technology (ICSICT) | 978-1-6654-6906-7/22/$31.00 ©2022 IEEE | DOI: 10.1109/ICSICT55466.2022.9963427

A Quantile-Based SUM/MAX Operating Method for Statistical Timing Analysis

Leilei Jin[1], Jiajie Xu[2], Wenjie Fu[3], Xiao Shi[4]

School of Electronic Science& Engineering, Southeast University, Nanjing 210096, China
[123]The National ASIC System Engineering Technology Research Center
[4]School of Computer Science and Engineering
* Email: {jinleilei, jiajiex, wenjfu, xshi}@seu.edu.cn

Abstract

Instead of expressing the delay distribution shape with complicated forms, we propose a quantile-based statistical SUM/MAX operating method by converting the distribution to several quantiles. Based on the numerical convolution, the SUM/MAX operations are converted to DNN with two groups of quantiles. The configuration of DNN models is discussed in this work, such as the hidden layer number and the transfer function. With 28 nm technology, the average errors of the DNN models for estimating the μ+3σ arrival time are less than 3% compared to the Monte Carlo simulations. The proposed method is more efficient than the NN-SSTA which needs to fit the shape of the whole distribution.

1. Introduction

Statistical static timing analysis (SSTA) is suitable for timing signoff analysis in advanced technology [1] [2][3]. Existing SSTA approaches can be classified into block-based SSTA [1][2] and path-based SSTA [3]. path-based SSTA analyzes each path in detail. In comparison, block-based SSTA is more efficient by using a breadth-first algorithm to analyze the timing graph. In block-based SSTA, for propagating arrival time distribution, the summation and maximum of two distributions are needed at each node in the circuit graph. With Clark's theory [7], the SUM/MAX results are usually calculated based on different forms such as the skew-normal models [1]. However, with technology scaling, the fluctuating process parameters cause complicated variations in electrical characteristics of the transistor and interconnect [8]. The distribution becomes non-gaussian at near-threshold regions [4][5]. It is hard to express the exact shape of the distribution and give the closed-form SUM/MAX results of several non-gaussian variables. The errors of the SUM/MAX results are unacceptable with the gaussian-based Clark assumption.

Actually, estimating the full shape of the delay distribution is non-trivial. To ensure the timing yield during the chip signoff, the most important information for the designer is the 99.86th percentile as the worst-case delay [9]. In addition, the worst-case, the mean (0.5^{th}), and the best-case delay (0.14^{th}) are also useful to provide a reasonable frequency for a target processor [9][10]. Inspired by the above demands, the nonnegative delay distribution of a circuit can be characterized by several quantiles. Based on the quantile-based delay model, the SUM/MAX operations of two delay distributions are converted to the DNN models, fed by several quantiles.

2. The SUM/MAX Operating Method

The circuit consists of primary inputs (PI), combinational cells (G_i), and primary outputs (PO). To propagate the arrival time, it needs to be transformed into a directed acyclic graph. Each pin of a cell is converted into a node, and nets connecting cells are converted into arcs. The arc from cell input to output is defined as the Cell-Arc, such as arc2 in Fig. 1. The arc converted by a net that connects two cells is defined as Net-Arc. The arrival time is defined as the time required from the primary inputs to each node. The arrival time at the primary outputs is considered as the delay of the entire circuit.

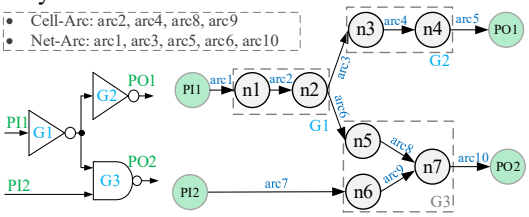

Figure 1. Examples of a circuit and the corresponding timing graph.

2.1 The Quantile-based SUM/MAX Operations

Suppose the arrival time at node n_i is AT_i and the Cell-Arc is T_{di} of the timing path. For the single-input cells, the arrival time at the output node can be calculated by (1). As shown in Fig. 2, the SUM of two distributions is equivalent to the convolution operation of the probability density functions (PDF) of two distributions in statistics.

$$AT_{i+1} = \mathrm{SUM}(AT_i, T_{di}) \quad (1)$$

Based on the discrete analysis, the PDF of the arrival time AT_{i+1}, represented by $P_{AT,i+1}$, can be calculated by (2) when the PDF of T_{di} is $P_{Td,i}$ and the PDF of AT_i is $P_{AT,i}$. The $P_{AT,i+1}(x)$ represents the probability when the arrival time of the output node i+1 is x. It is widely known that the PDF is the derivative of the cumulative distribution function (CDF). With enough discrete points, the CDF of a distribution $F(x)$ can be approximated by

978-1-6654-6906-7/22/$31.00 © 2022 IEEE
Authorized licensed use limited to: Chinese University of Hong Kong. Downloaded on November 22,2026 at 12:59:36 UTC from IEEE Xplore. Restrictions apply.

a combination of piecewise linear functions. Accordingly, the probability of the distribution at $n\sigma$ can be approximated as the linear summation of the derivative of several neighboring quantiles as shown in (3).

$$P_{AT,i+1}(x) = \sum_{t=-\infty}^{\infty} P_{AT,i}(t) P_{Td,i}(x-t) \quad (2)$$

$$\begin{aligned} P(n\sigma) &= \frac{d}{dx}\big(F(x)\big)\Big|_{x=n\sigma} \\ &= \frac{1}{2}\frac{F(n\sigma)-F((n-1)\sigma)}{n\sigma-(n-1)\sigma} + \frac{1}{2}\frac{F((n+1)\sigma)-F(n\sigma)}{(n+1)\sigma-n\sigma} \\ &\approx (w_1(n+1)\sigma + w_2 n\sigma)^{-1} + (w_3(n+1)\sigma + w_4 n\sigma)^{-1} \end{aligned} \quad (3)$$

For a more detailed characterization, seven quantiles $(-3\sigma, -2\sigma, -\sigma, \mu, \sigma, 2\sigma, 3\sigma)$ are chosen to stand for the distribution, which are 0.14th, 2.28th, 15.87th, 50th, 84.13th, 97.72th, and 99.86th. Based on these quantiles, the probabilities of AT_i and T_{di} are $P_{AT,i}(j\sigma)$ and $P_{Td,i}(k\sigma)$ where j and k range from -3 to 3, respectively. As the result of discrete convolution, the minimum number of quantiles is 13 when the distributions of AT_i and T_{di} are the same. The maximum number of quantiles is 49 when the distributions of AT_i and T_{di} are quite different. Hence, $P_{AT,i+1}$ of $m\sigma$ can be represented by (4), where $m\sigma$ is a floating number ranging from the -3σ of AT_i to the 3σ of T_{di}.

$$P_{AT,i+1}(m\sigma) = \sum_{j=1}^{7}\sum_{k=1}^{7} P_{AT,i}(j\sigma) P_{Td,i}(k\sigma) \quad (4)$$

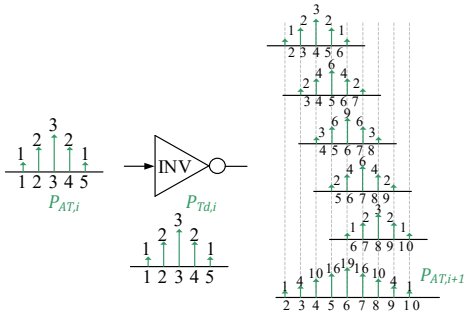

Figure 2. The statistical SUM operation of the discrete probability distribution.

The arrival time at the output node of a multi-input cell, such as NAND, is the maximum of the arrival time from each Cell-Arc. As shown in Fig. 3, the arrival time ($AT1_{i+1}$) stimulated by IN1 can be calculated by summarizing $AT1_i$ and $Td1_i$ of Cell-Arc (A1→ZN), recorded as SUM$(AT1_i, Td1_i)$. Similarly, $AT2_{i+1}$ (A2→ZN) can be calculated by SUM$(AT2_i, Td2_i)$. With an input transition on IN1 or IN2, the arrival time at ZN is the result of the MAX operation, briefly AT_{i+1} as shown in (5). Similar to the SUM operation, the MAX of two distributions is equivalent to the convolution operation of the PDF of $AT1_{i+1}$ and $AT2_{i+1}$ as shown in (6). The probability of the distribution at $m\sigma$ can also be approximated using (7).

$$\begin{aligned} AT_{i+1} &= \mathrm{MAX}\big(\mathrm{SUM}(AT1_i, Td1_i),\ \mathrm{SUM}(AT2_i, Td2_i)\big) \\ &= \mathrm{MAX}(AT1_{i+1}, AT2_{i+1}) \end{aligned} \quad (5)$$

$$P_{AT,i+1}(x) = \sum_{t=-\infty}^{\infty} P_{AT1,i+1}(t) P_{AT2,i+1}(x-t) \quad (6)$$

$$P_{AT,i+1}(m\sigma) = \sum_{j=1}^{7}\sum_{k=1}^{7} P_{AT1,i+1}(j\sigma) P_{AT2,i+1}(k\sigma) \quad (7)$$

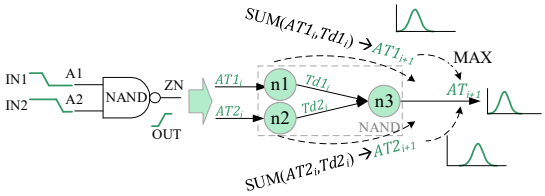

Figure 3. The statistical MAX operation of NAND.

2.2 The DNN-based Predicting Method

As shown in Fig. 4, a deep neural network model is used to predict the convolution results. Taken the expression in (3) as the atomic operation for the DNN. The $n\sigma$ quantiles of the delay distribution are taken as the training data where n is an integer ranging from -3 to 3. After multiply accumulation, the input is transformed through the activation function to get the desired output. Taken f_{tran1} as the transfer function from $n\sigma$ to the PDF of output, the (3) can be converted to (8) where w and b are the regression coefficients. Similarly, $P_{Td,i}$ of Cell-Arc can be obtained. Based on $P_{AT,i}$ and $P_{Td,i}$, the PDF of $P_{AT,i+1}$in (4) is converted to (9).

$$P_{AT,i}(n\sigma) = f_{tran1}\big(\sum_{k=1}^{7} wk\sigma + b\big) \quad (8)$$

$$\begin{aligned} P_{AT,i+1}(m\sigma) \approx f_{tran3}\big(\sum w f_{tran2}\big(\sum (w_j P_{AT,i}(m\sigma) \\ + w_k P_{Td,i}(m\sigma)) + b\big) + b\big) \end{aligned} \quad (9)$$

The $n\sigma$ of the convolution result can be estimated from several adjacent quantiles, for example, $n\sigma|_{n=1} \approx \sum(w_j P(m_i\sigma),\ m_i \in \{0.5,\ 0.8,\ 1.2,\ 1.5\}$. Hence, the $n\sigma$ can be represented by (8) considering the form of neurons.

$$n\sigma = f_{tran4}\big(\sum w_i P_{AT,i+1}(m\sigma) + b\big) \quad (10)$$

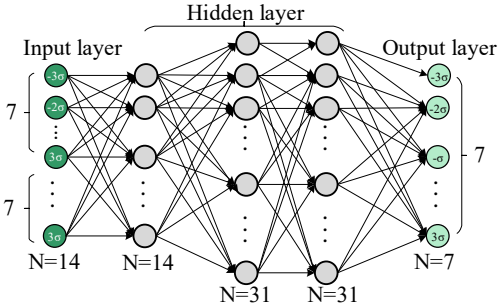

Figure 4. The deep neural network structure for the statistical SUM/MAX operations.

The SUM/MAX operations have two distributions as inputs and one distribution as output. Each distribution is characterized by seven quantiles and each of which corresponds to a neuron. Hence, the DNN is configured with 14 neurons in the input layer and 7 neurons in the output layer. Combining (8) ~ (10), the DNN contains 3 hidden layers, corresponding to the calculation of $P_{AT,i}(n\sigma)$, $P_{AT,i}(j\sigma)P_{Td,i}(k\sigma)$, and$P_{AT,i+1}(m\sigma)$. The first hidden layer contains 14 neurons and the second and the third hidden layer both contain at least 13 neurons, and up to 49 neurons. f_{tran1}, f_{tran2}, f_{tran3}, and f_{tran4} are the transfer functions, and w, w_j, w_k and b are the weight coefficients and offset values of each layer.

Authorized licensed use limited to: Chinese University of Hong Kong. Downloaded on November 22,2026 at 12:59:36 UTC from IEEE Xplore. Restrictions apply.

3. Evaluation

The supply voltage is set to be 0.5V as the near-threshold region. The DNN models are tested using the ISCAS85 benchmark based on SMIC 28 nm PDK.

The TANSIG transfer function is used in the DNN to connect the input and the three hidden layers effectively [11]. Since the prediction results sometimes transcend the training space, the PURELIN transfer function is used in the model's output layer [11]. The optimal solutions of each layer can be iteratively calculated by training methods, such as gradient descent (GD), and Levenberg-Marquardt (LM) [12]. Using the 'TANSIG-TANSIG-PURELIN' transfer functions [11], the influence of choosing different training methods is shown in Fig. 5. LM outperforms other training functions in prediction accuracy which is chosen as our training function. Fig. 6 illustrates the prediction errors and training time of DNN with different combinations of neurons in the hidden layer. The training errors of the SUM/MAX exhibit a quick diminishing trend as the number of neurons increases. However, when the node configuration increases to 14-31-31, the error remains steady. In addition, the training overhead is in proportion to the number of neurons. When the neurons are configured as 18-39-39, significant storage/compute overheads are incurred for training the DNN models.

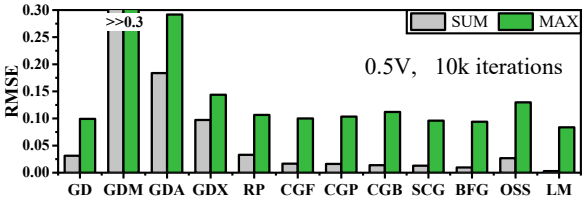

Figure 5. Comparison of training errors of the DNN models with different training methods

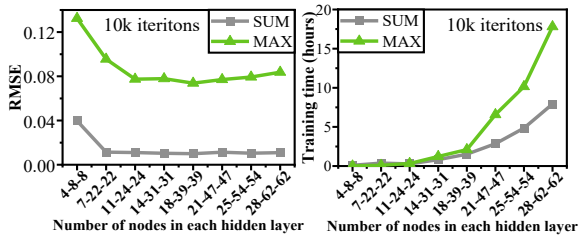

Figure 6. Comparison of training error and time consumption of the DNN model with different combinations of neuron numbers

As shown in Fig. 7, taking NANDX1 as an example, the MAX results using the DNN model are compared with using the NN-SSTA model [4], the MC simulations, and the LVF model [6]. Although NN-SSTA can obtain the curve of the distribution, it adds computing complexity based on sampling. With efficient accuracy, our model predicts accurate $n\sigma$ quartiles of arrival time, instead of the specific distribution curve. Furthermore, as shown in Table I and Fig, 8, the accuracy of our model to predict the $\mu+3\sigma$ of the arrival time is higher than the LVF method, especially in lower voltage.

4. Summary

This paper presents a DNN-based method for estimating the SUM/MAX results with the quantile-based delay distribution. Based on the ISCAS85 benchmarks, the proposed method is more precise than the LVF method and more efficient than NN-SSTA.

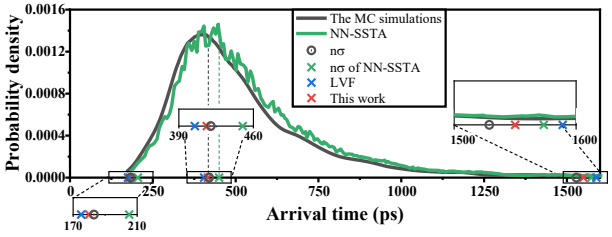

Figure 7. Comparison of the statistical MAX accuracy of NANDX1 based on the DNN model.

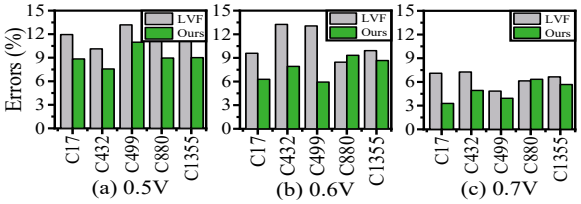

Figure 8. Comparison of the prediction errors of +3σ arrival time at different supply voltages.

Table I. The prediction errors of arrival time.

Bench	Number of SUM/MAX	Errors of μ (%)		Errors of $\mu-3\sigma$ (%)		Errors of $\mu+3\sigma$ (%)	
		LVF[6]	Ours	LVF[6]	Ours	LVF[6]	Ours
C17	32/8	2.84	3.10	11.23	6.59	11.95	8.84
C432	950/320	2.99	3.26	12.37	4.92	10.13	7.57
C499	1404/476	4.63	1.84	12.09	2.93	13.19	10.98
C880	1318/455	2.87	2.13	5.19	3.33	13.41	8.96
C1355	1674/574	4.82	2.64	7.38	5.67	15.28	9.01
Average		3.63	2.59	9.65	4.69	12.79	9.07

References

[1] Ramprasath S, Vijaykumar M, Vasudevan V. IEEE Transactions on Very Large Scale Integration (VLSI) Systems, 24(6), p2359, (2015)

[2] Fu W, Jin L, et al. IEEE Access, 8, p.197194, (2020).

[3] Kahng A B, Mallappa U, et al. ICCD. IEEE, p.603 (2018).

[4] Savari M A, Jahanirad H. Expert Systems with Applications, 149, p113309, (2020).

[5] Jin L, Fu W, Yan H, et al. IEEE Transactions on Circuits and Systems II: Express Briefs, 69(6), p2932, (2022).

[6] Rita M, Aru S, Manish B. Journal of Physics: Conference Series. IOP Publishing, 1706(1), p012081, (2020).

[7] Clark C E. Operations Research, 1961, 9(2): 145-162.

[8] Huynh-Bao T, Ryckaert J, Tőkei Z, et al. IEEE Transactions on Very Large Scale Integration (VLSI) Systems, 25(5): 1669-1680, (2017).

[9] Shah A, Nayyar R, Sinha A. 2019 IEEE 37th VLSI Test Symposium (VTS). IEEE, 1-6, (2019).

[10] Fu W, Jin L, Ling M, et al. 2020 57th ACM/IEEE Design Automation Conference (DAC). IEEE, 1-6 (2020).

[11] Dorofki M, Elshafie A H, Jaafar O, et al. International Proceedings of Chemical, Biological and Environmental Engineering, 33: 39-44, (2012).

[12] Mukherjee I, Routroy S. Expert Systems with Applications, 39(3): 2397-2407, (2012).

Authorized licensed use limited to: Chinese University of Hong Kong. Downloaded on November 22,2026 at 12:59:36 UTC from IEEE Xplore. Restrictions apply.